Original Article

Institution of MECHANICAL ENGINEERS
Journal of MECHANICAL ENGINEERING SCIENCE

Proc IMechE Part C:
J Mechanical Engineering Science
227(5) 935–945

DOI: 10.1177/0954406212452064
pic.sagepub.com
SAGE

Aeolian vibration of a single conductor with a Stockbridge damper

Oumar Barry, Donatus CD Oguamanam and Der Chyan Lin

Abstract

The planar vibrational response of a single conductor with an attached Stockbridge damper is investigated. The mathematical model accounts for the two-way coupling between the conductor and the damper, the flexural rigidity of both the damper and the conductor, and the mass of the two counterweights of the damper. Hence, the dynamic behaviors of the damper and conductor are simultaneously assessed. Both free and forced vibration analyses are implemented via the use of a finite element code developed in MATLAB. The results of the force vibration analyses show that the effectiveness of Stockbridge dampers depends on their location, mass, and excitation frequency.

Keywords

Aeolian vibration, Stockbridge damper, Strouhal frequency, messenger cable, transmission line

Date received: 14 February 2012; accepted: 28 May 2012

Introduction

Aeolian vibration of transmission line conductor arises from alternating wind forces that are caused by vortex shedding. The frequency of vibration, also called Strouhal frequency, is observed in a specific range, usually between 3 and 50 Hz with a wind speed of 1–7 m/s.[1] Aeolian vibration imperils the life of transmission lines and, if uncontrolled, could cause serious accidents and/or considerable economic loss. A method to eradicate the vibration is the use of damping devices, such as the Stockbridge damper.

This subject has attracted several investigations, one of the earliest being by Claren and Diana[2] who showed that the physical model of the conductor is similar to an Euler–Bernoulli beam under the action of an axial load (i.e. design tension). This model was used by Barbieri et al.[3] and the equation of motion was solved using the Galerkin-weighted-residual method. The results of the free vibration analysis were experimentally validated.

Dhotard et al.[4] also employed the mathematical model of Claren and Diana[2] to examine the dynamics of a single-conductor vibration with dampers. They concluded that damper locations had more effect on strains at higher frequencies than at lower ones. The amplitudes of vibration were observed to depend solely on the location of the damper. The investigation by Nigol and Houston[5] on single conductor advised against positioning dampers at points of symmetry along the span of the conductor (such as 1/4, 1/3, 1/2, etc.). For single-damper conductors under normal design tensions, a damper location between 1.2 and 1.8 m was suggested for frequencies of 40–50 Hz; for longer span and/or higher tension, two dampers were suggested with one located at a distance between 2.4 and 3.6 m from one terminal, and the other located at between 1.0 and 2.2 m from the second terminal.

Krispin[6] outlined the advantages of a Stockbridge-type vibration damper with a low-mass clamp over a conventional Stockbridge vibration damper with a bolted clamp. It was shown, analytically and experimentally, that the large-mass clamp of the conventional Stockbridge was a disadvantage in regard to damping high-frequency vibrations of small diameter optical ground wires. The energy dissipated by a Stockbridge damper was dependent upon vibration frequency and the displacement amplitudes of the damper clamp.[7] These factors were influenced by the location of the damper.

The wind force acting on a conductor was the concern of Diana et al.[8] The transmission line vibration was observed to be identical to that of a rigid cylinder since the wind force was proportional to the diameter and the length of the conductor and the square of the wind velocity. These conclusions were

Department of Mechanical and Industrial Engineering, Ryerson University, Toronto, Canada

Corresponding author:
Donatus CD Oguamanam, Department of Mechanical and Industrial Engineering, Ryerson University, Toronto, Ontario M5B 2K3, Canada.
Email: doguaman@ryerson.ca

corroborated by Bishop and Hassan[9] and Bearman and Currie.[10] The lift force led the displacement by a phase angle ranging from 0° to 180° during resonance. Griffin and Koopmann[11] experimentally demonstrated that the lift coefficient depended on the ratio of the maximum amplitude of vibration to the diameter of a rigid cylinder. A maximum lift coefficient of 0.55 corresponded to a maximum peak-to-peak vibration amplitude of 0.55 diameter.

The ratio of the vibration amplitude at the damper clamp to that of the free span is of interest in the energy balance method. Claren and Diana[2] determined the ratio using the summation of assumed modes technique, while the techniques of wave propagation and matrix transfer are employed in Hagedorn[12] and Hardy and Noiseux,[13] respectively. Other modeling concepts that have been explored include the use of statistical methods by Noiseux et al.[14] and the approach of multiphysics as presented by Tsui[15] in which non-linear mechanics, fluid dynamics, and aeroelasticity are simultaneously employed.

A different approach to model the planar vibration of a single-damper conductor is adopted in this study. The proposed model directly incorporates the two-way coupling between the conductor and the Stockbridge damper. It includes the flexural rigidities of the conductor and the messenger, and it permits the use of either symmetric or asymmetric Stockbridge dampers so that the influence of unbalance in the counterweights can be readily investigated.

Mathematical model

Description of the system

The length of the conductor is denoted by L_c. The distance of the damper from the nearest terminal is denoted by L_d. Figure 1 is a close-up view of the counterweights of the damper. The equations of motion of the system are determined using the energy method. The position vectors employed in the derivation of the kinetic and potential energies are identified in Figure 1 for the right-hand side counterweight only for brevity. The corresponding vectors for the left-hand side counterweight merely have the subscript r replaced by l to denote the left side. The clamp is assumed to be rigid and fixed to the conductor, which implies that the height h (length of the clamp plate) is always perpendicular to the conductor at its point of attachment. Figure 2 depicts a schematic of a finite element of the conductor with a damper.

Equations of motion

A reference frame F_0 is attached to one end of the conductor. Using Figure 1, a frame F_1 is attached to the clamp of the damper, while frames F_2 and F_3 are, respectively, attached to the right-hand side and left-hand side counterweights. Frame F_1' is the translation of frame F_1 attached at the point of contact of the clamp and messenger. The set of planar unit vectors

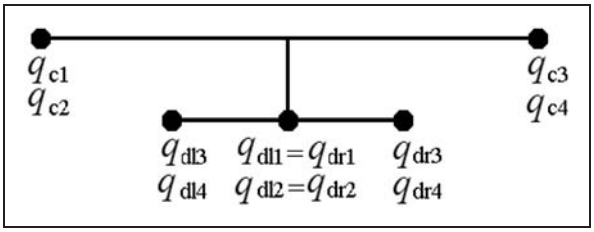

Figure 2. Schematic of finite element of the conductor with damper.

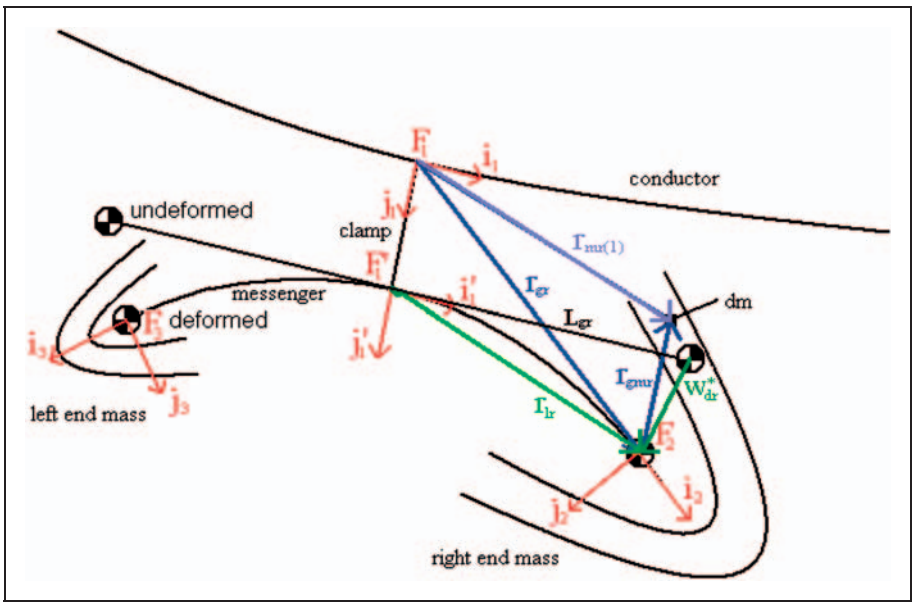

Figure 1. A close-up view of the damper.

of frame F_1' is $\{\mathbf{i}_1', \mathbf{j}_1'\}$ and that of frame F_α for $\alpha = 1, 2, 3$ is $\{\mathbf{i}_\alpha, \mathbf{j}_\alpha\}$.

The position vector of a deformed differential element of the conductor is written as

$$\mathbf{r}_c(x, t) = x\mathbf{i}_0 + w_c(x, t)\mathbf{j}_0 \tag{1}$$

where $w_c(x, t)$ denotes the conductor transverse displacement. If the point of attachment of the damper is L_d, then the position vector of the damper location is given as

$$\mathbf{r}_c^* = L_d\mathbf{i}_0 + w_c(L_d, t)\mathbf{j}_0 \tag{2}$$

The position vector of the right-end counterweight with respect to the reference frame F_0 is given as

$$\mathbf{r}_{mr(0)} = \mathbf{r}_{mr(1)} + \mathbf{r}_c^* \tag{3}$$

where

$$\begin{aligned}\mathbf{r}_{mr(1)} &= \mathbf{r}_{gr} + \mathbf{r}_{gmr}\\ \mathbf{r}_{gr} &= \mathbf{r}_h + \mathbf{r}_{lr}\\ \mathbf{r}_{lr} &= L_{gr}\mathbf{i}_1 + w_{dr}^*\mathbf{j}_1\\ \mathbf{r}_{ll} &= -L_{gl}\mathbf{i}_1 + w_{dl}^*\mathbf{j}_1\end{aligned}$$

where

$$\begin{aligned}w_{dr}^* &= w_{dr}(L_{dr}, t)\\ w_{dl}^* &= w_{dl}(L_{dl}, t)\end{aligned}$$

where $w_{dr}(\boldsymbol{L}_{dr}, t)$ and $w_{dr}(\boldsymbol{L}_{dl}, t)$ denote the messenger transverse displacement at the right and left ends of the damper, respectively, and $\mathbf{r}_h$ the vector from frame F_1 to frame F_1'. Here, $\mathbf{r}_{mr(1)}$ represents the position of the right-end counterweight with respect to frame F_1, $\mathbf{r}_{lr}$ the vector from frame F_1' to frame F_2, and $\mathbf{r}_{ll}$ the vector from frame F_1' to frame F_3. L_{gr} and L_{gl} denote the length of the damper cable on the right and left sides, respectively. The position vector $\mathbf{r}_{mr(0)}$ can now be expressed

$$\mathbf{r}_{mr(0)} = \mathbf{r}_{gr} + \mathbf{r}_{gmr} + \mathbf{r}_c^* \tag{4}$$

Similarly, the position vector of the counterweight on the left side can be written as

$$\mathbf{r}_{ml(0)} = \mathbf{r}_{gl} + \mathbf{r}_{gml} + \mathbf{r}_c^* \tag{5}$$

The position vectors of the messenger on the right and left sides are

$$\mathbf{r}_{mmr} = \mathbf{r}_c^* + \mathrm{r}_h + x_{mm}\mathbf{i}_1 + w_{dr}(x_{mm}, t)\mathbf{j}_1 \tag{6}$$

$$\mathbf{r}_{mml} = \mathbf{r}_c^* + \mathbf{r}_h + x_{mm}\mathbf{i}_1 + w_{dl}(x_{mm}, t)\mathbf{j}_1 \tag{7}$$

where

$$w_c^* = w_c(L_d, t)$$

The corresponding velocities are

$$\dot{\mathbf{r}}_c = \dot{w}_c(x, t)\mathbf{j}_0 \tag{8}$$

$$\dot{\mathbf{r}}_c^* = \dot{w}_c^*(x, t)\mathbf{j}_0 \tag{9}$$

and

$$\dot{\mathbf{r}}_{mr(1)} = \dot{\theta}_1 h\mathbf{i}_1 + L_{gr}\dot{\theta}_1\mathbf{j}_1 + \dot{w}_{dr}^*\mathbf{j}_1 + w_{dr}^*\dot{\theta}_1 + \omega_r \times \mathbf{r}_{gmr} \tag{10}$$

$$\dot{\mathbf{r}}_{ml(1)} = \dot{\theta}_1 h\mathbf{i}_1 - L_{gl}\dot{\theta}_1\mathbf{j}_1 + \dot{w}_{dl}^*\mathbf{j}_1 + w_{dl}^*\dot{\theta}_1 + \omega_l \times \mathbf{r}_{gml} \tag{11}$$

where

$$\omega_r = (\dot{\theta}_1 + \dot{\theta}_2)\mathbf{k} \text{ and } \omega_l = (\dot{\theta}_1 + \dot{\theta}_3)\mathbf{k}$$

where $\dot{\theta}_1$ is the angular speed of frame F_1 with respect to F_0 and $\dot{\theta}_2$ and $\dot{\theta}_3$ the angular speeds of frames F_2 and F_3 with respect to F_0, respectively. The length of the damper clamp is denoted by h.

Assuming small rotation and neglecting higher-order terms, the system kinetic energy may be written as

$$KE = T_c + T_{mr} + T_{ml} + T_{mmr} + T_{mml}$$

where

$$T_c = \frac{(\rho A)_c}{2}\int_0^{L_c} \dot{\mathbf{r}}_c \cdot \dot{\mathbf{r}}_c \mathrm{d}x \tag{12}$$

$$\begin{aligned}T_{mr} = \frac{1}{2}m_{dr}\Big\{&\dot{w}_c^{*2} + 2\dot{w}_c^*(\dot{\theta}_1 L_{gr} + \dot{w}_{dr}^*)\\ &+ \dot{\theta}_1^2(h^2 + L_{gr}^2) + 2L_{gr}\dot{w}_{dr}^*\dot{\theta}_1 + \dot{w}_{dr}^{*2}\Big\}\\ &+ \frac{1}{2}I_{dr}(\dot{\theta}_1 + \dot{\theta}_2)^2\end{aligned} \tag{13}$$

$$\begin{aligned}T_{ml} = \frac{1}{2}m_{dl}\Big\{&\dot{w}_c^{*2} + 2\dot{w}_c^*(-\dot{\theta}_1 L_{gl} + \dot{w}_{dl}^*)\\ &+ \dot{\theta}_1^2(h^2 + L_{gl}^2) - 2L_{gl}\dot{w}_{dl}^*\dot{\theta}_1 + \dot{w}_{dl}^{*2}\Big\}\\ &+ \frac{1}{2}I_{dl}(\dot{\theta}_1 + \dot{\theta}_3)^2\end{aligned} \tag{14}$$

$$\begin{aligned}T_{mmr} = &\frac{1}{2}m_{mr}(\dot{w}_c^{*2} + (\dot{\theta}_1 h)^2)\\ &+ \frac{1}{2}(\rho A)_{mr}\int_0^{L_{gr}}\Big\{2\dot{w}_c^*\dot{w}_{dr} + 2x_{mr}\dot{\theta}_1\dot{w}_{dr} + \dot{w}_{dr}^2\Big\}\mathrm{d}x\\ &+ \frac{1}{2}(\rho A)_{mr}(\dot{w}_c^*\dot{\theta}_1 L_{gr}^2 + \frac{2}{3}\dot{\theta}_1^2 L_{gr}^3)\end{aligned} \tag{15}$$

$$T_{\mathrm{mml}} = \frac{1}{2} m_{\mathrm{ml}} (\dot{w}_{\mathrm{c}}^{*2} + (\dot{\theta}_1 h)^2) + \frac{1}{2} (\rho A)_{\mathrm{ml}} \int_0^{L_{\mathrm{gl}}} \left\{ 2\dot{w}_{\mathrm{c}}^{*} \dot{w}_{\mathrm{dl}} - 2x_{\mathrm{ml}} \dot{\theta}_1 \dot{w}_{\mathrm{dl}} + \dot{w}_{\mathrm{dl}}^2 \right\} \mathrm{d}x - \frac{1}{2} (\rho A)_{\mathrm{ml}} (\dot{w}_{\mathrm{c}}^{*} \dot{\theta}_1 L_{\mathrm{gl}}^2 + \frac{2}{3} \dot{\theta}_1^2 L_{\mathrm{gl}}^3) \quad (16)$$

The moments of inertia of the right- and left-side dampers are denoted by $\boldsymbol{I}_{\mathrm{dr}}$ and $\boldsymbol{I}_{\mathrm{dl}}$, respectively, while m_{dr} and m_{dl}, respectively, denote the mass of the right- and left-side dampers. Furthermore, ρ and A, respectively, represent the density and the cross-sectional area.

The system total potential energy is given as

$$PE = \frac{1}{2} (EI)_{\mathrm{c}} \int_0^{L_{\mathrm{c}}} \frac{\partial^2 w_{\mathrm{c}}^2}{\partial x^2} \mathrm{d}x - \frac{1}{2} T \int_0^{L_{\mathrm{c}}} \frac{\partial w_{\mathrm{c}}^2}{\partial x} \mathrm{d}x + \frac{1}{2} (EI)_{\mathrm{mr}} \int_0^{L_{\mathrm{gr}}} \frac{\partial w_{\mathrm{mr}}^2}{\partial x} \mathrm{d}x + \frac{1}{2} (EI)_{\mathrm{ml}} \int_0^{L_{\mathrm{gl}}} \frac{\partial w_{\mathrm{ml}}^2}{\partial x} \mathrm{d}x \quad (17)$$

where E is the Young's modulus of elasticity and $\boldsymbol{I}_{\mathrm{c}}$ the area moment of inertia of the conductor.

The kinetic and potential energies are employed in the Hamilton's principle to derive the equations of motion of the element of the conductor with a damper (see Barry[16] for more details). The set of finite-dimensional system equations of motion is obtained using the finite element model. The finite-element of the conductor with the damper is depicted in Figure 2. It is composed of fives nodes, two for the conductor and three for the messenger.

The transverse deformations are interpolated using cubic Hermite polynomials. The shape functions of the transverse deformation N_1, N_2, N_3, and N_4 are given as

$$N_1 = 1 - 3\frac{\xi^2}{L_e^2} + 2\frac{\xi^3}{L_e^3} \quad N_2 = \xi - 2\frac{\xi^2}{L_e} + \frac{\xi^3}{L_e^2}$$
$$N_3 = 3\frac{\xi^2}{L_e^2} - 2\frac{\xi^3}{L_e^3} \quad N_4 = -\frac{\xi^2}{L_e} + \frac{\xi^3}{L_e^2} \quad (18)$$

where L_e denotes the length of the element. The displacement of the conductor, the right-side damper, and the left-side damper are written as follows

$$\mathbf{w}_{\mathrm{c}} = \mathbf{N}_{\mathrm{c}}^T \mathbf{q}_{\mathrm{c}}$$
$$\mathbf{w}_{\mathrm{dr}} = \mathbf{N}_{\mathrm{dr}}^T \mathbf{q}_{\mathrm{dr}}$$
$$\mathbf{w}_{\mathrm{dl}} = \mathbf{N}_{\mathrm{dl}}^T \mathbf{q}_{\mathrm{dl}} \quad (19)$$

where the $\mathbf{q}$s represents element displacement vectors. The subscripts c, dr, and dl denote the conductor, the damper on the right, and the damper on the left, respectively.

The nodal displacement vectors of the conductor element, right-side damper element, and left-side damper element can be written as

$$\mathbf{q}_{\mathrm{c}}^T = \{ q_{\mathrm{c1}} \quad q_{\mathrm{c2}} \quad q_{\mathrm{c3}} \quad q_{\mathrm{c4}} \}$$
$$\mathbf{q}_{\mathrm{dr}}^T = \{ q_{\mathrm{dr1}} \quad q_{\mathrm{dr2}} \quad q_{\mathrm{dr3}} \quad q_{\mathrm{dr4}} \}$$
$$\mathbf{q}_{\mathrm{dl}}^T = \{ q_{\mathrm{dl1}} \quad q_{\mathrm{dl2}} \quad q_{\mathrm{dl3}} \quad q_{\mathrm{dl4}} \}$$

and the element finite-dimensional equations of motion may be expressed as

$$\begin{bmatrix} \mathbf{M}_{\mathrm{cc}} & \mathbf{M}_{\mathrm{cr}} & \mathbf{M}_{\mathrm{cl}} \\ \mathbf{M}_{\mathrm{rc}} & \mathbf{M}_{\mathrm{rr}} & 0 \\ \mathbf{M}_{\mathrm{lc}} & 0 & \mathbf{M}_{\mathrm{ll}} \end{bmatrix} \begin{Bmatrix} \ddot{\mathbf{q}}_{\mathrm{c}} \\ \ddot{\mathbf{q}}_{\mathrm{dr}} \\ \ddot{\mathbf{q}}_{\mathrm{dl}} \end{Bmatrix} + \begin{bmatrix} \mathbf{K}_{\mathrm{cc}} & 0 & 0 \\ 0 & \mathbf{K}_{\mathrm{rr}} & 0 \\ 0 & 0 & \mathbf{K}_{\mathrm{ll}} \end{bmatrix} \begin{Bmatrix} \mathbf{q}_{\mathrm{c}} \\ \mathbf{q}_{\mathrm{dr}} \\ \mathbf{q}_{\mathrm{dl}} \end{Bmatrix} = \int_0^{L_{\mathrm{c}}} F(t) \mathbf{N}_{\mathrm{c}} \, \mathrm{d}x \quad (20)$$

where $F(t) = F_l * \sin(\Omega * t)$ and Ω denotes the forcing frequency. The components of the inertia and stiffness matrices are listed in the Appendix.

Numerical simulation

A free vibration analysis was performed on a single-damper conductor using pinned–pinned boundary condition. The following parameters were employed: $EI_{\mathrm{c}} = 3.19\,\mathrm{N/m^2}$; $EI_{\mathrm{dr}} = 0.5\,\mathrm{N/m^2}$; $EI_{\mathrm{dl}} = 0.5\,\mathrm{N/m^2}$; $m_{\mathrm{dr}} = 4\,\mathrm{kg}$ and $m_{\mathrm{dl}} = 2.75\,\mathrm{kg}$; $\rho A_{\mathrm{mr}} = \rho A_{\mathrm{ml}} = 0.2\,\mathrm{kg/m}$; $L_{\mathrm{dr}} = L_{\mathrm{dl}} = 0.2\,\mathrm{m}$; clamp height, $h = 0.05\,\mathrm{m}$. The damper was located at a distance of 4.1 m from the left-end of the conductor whose span length is 13.375 m. To verify the model, a zero conductor tension is assumed in order to examine the effect of damper properties on the system natural frequency independent of tension. The first 10 natural frequencies obtained from a MATLAB code are given in Table 1 which also shows the corresponding results obtained using ANSYS. The conductor and messenger were modeled in ANSYS using 20 and 10 BEAM3 elements, respectively. The two counterweights at the ends of the messengers were modeled as MASS21 elements (which are two-dimensional masses with rotational inertia). The clamp was modeled as BEAM3 and its mass is negligible when compared to that of the conductor and the messenger. The maximum percentage error is 4.38%. The fifth mode is the first mode at which significant deformation of the damper was observed. A close-up view is illustrated in Figure 3.

The simulation results reported hereinafter were based on $240/40\,\mathrm{mm^2}$ ACSR(26/7) conductors and the parameters were obtained from EPRI.[1] The span length $L = 372\,\mathrm{m}$, tension was fixed at 20% RTS (rated tensile strength), the amplitude of the applied wind force $F_{\mathrm{l}} = 0.18522\,\mathrm{N/m}$, and the forcing frequency $\Omega = 9.53\,\mathrm{Hz}$.

Effect of damper mass

The damper was positioned at a distance $L_d = 1.1$ m and the response along the conductor was determined by varying the mass of each counterweight from 0.86 to 4 kg. Figure 4 shows that the peak-to-peak vibration amplitudes of both counterweights, Y_r and Y_l, increase with increasing damper mass, with the smaller counterweight mass exhibiting the largest non-dimensionalized peak-to-peak amplitude. The non-dimensionalization is with respect to the conductor diameter.

Table 1. Comparison of ANSYS and MATLAB natural frequencies of the conductor with damper for $L = 13.375$ m, $L_d = 4.1$ m, and $T = 0$ N.

	Natural frequency (Hz)	
Mode	ANSYS	MATLAB
1	0.0531	0.0537
2	0.1538	0.1502
3	0.3736	0.3642
4	0.6123	0.6296
5	0.8439	0.8462
6	1.2477	1.2301
7	1.5733	1.6421
8	2.0734	2.0814
9	2.3401	2.5789
10	2.8464	2.9036

The maximum peak-to-peak response of the conductor at each location of the damper within the optimal range is illustrated in Figure 5 for various combinations of counterweight masses. The light-mass damper yields smaller peak-to-peak displacement when compared to the corresponding heavy-mass damper. Further, it appears that it is best, for a given total mass combination, to locate the smaller counterweight mass to the right side, closer to the mid-span, because this arrangement dissipates the most energy.

Effect of the forcing frequency

To examine the effect of excitation frequency, a damper was placed at a distance $L_d = 0.898$ m. The mass of the counterweight on the right-hand side 0.86 kg while that on the left-hand side 1.5 kg. The other properties of the damper were identical to those used in the validation exercise. The results are depicted in Figure 6. The maximum non-dimensionalized amplitude of vibration, Y_{max}, and the non-dimensional vibration amplitude of the mid-span, Y_{mid}, are observed to decrease with increasing excitation frequency. The non-dimensional vibration amplitude of the second and penultimate nodes, i.e. those nodes that are adjacent to the edge nodes, Y_2 and Y_f, remain slightly constant as the frequency varies. The lack of exact match between the plots is due to the asymmetry in the problem. Further, this asymmetry might explain the absence of an exact match in the displacement amplitudes of the second and penultimate nodes.

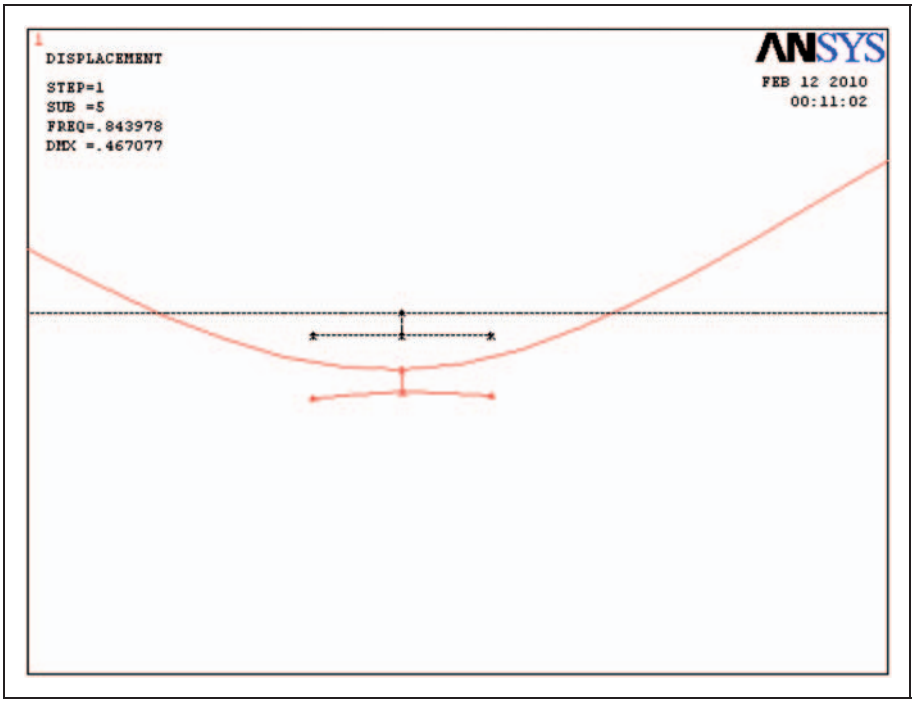

Figure 3. A close-up view of the fifth mode, the first time significant deformation is observed in the damper.

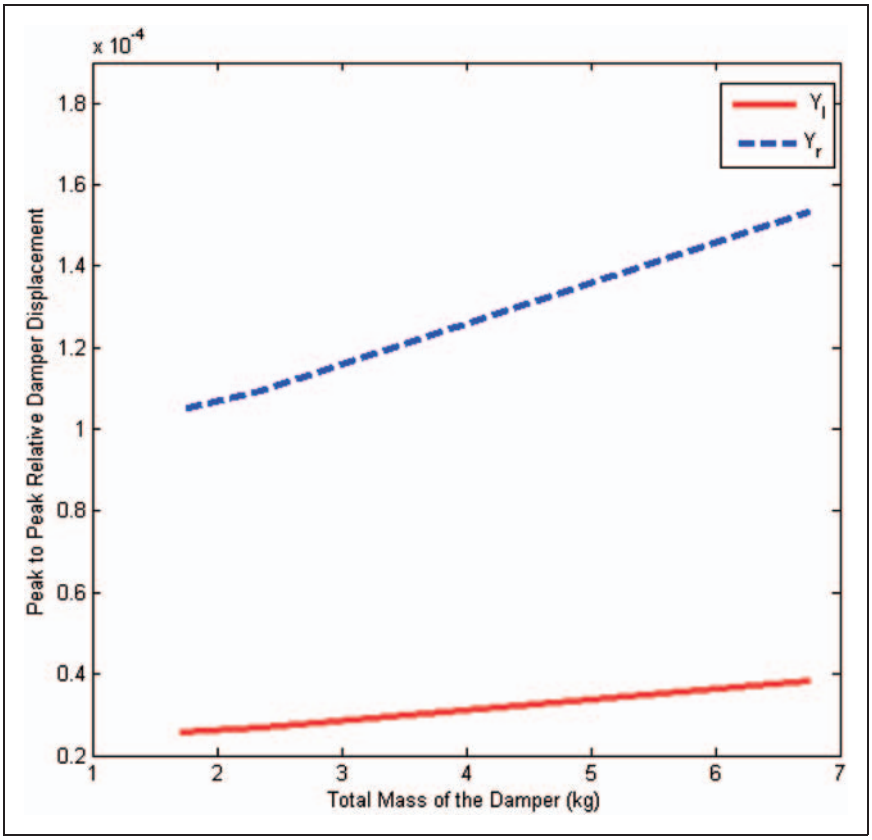

Figure 4. Effect of the total damper mass on the damper response for $f = 9.53$ Hz and $L_d = 1.1$ m.

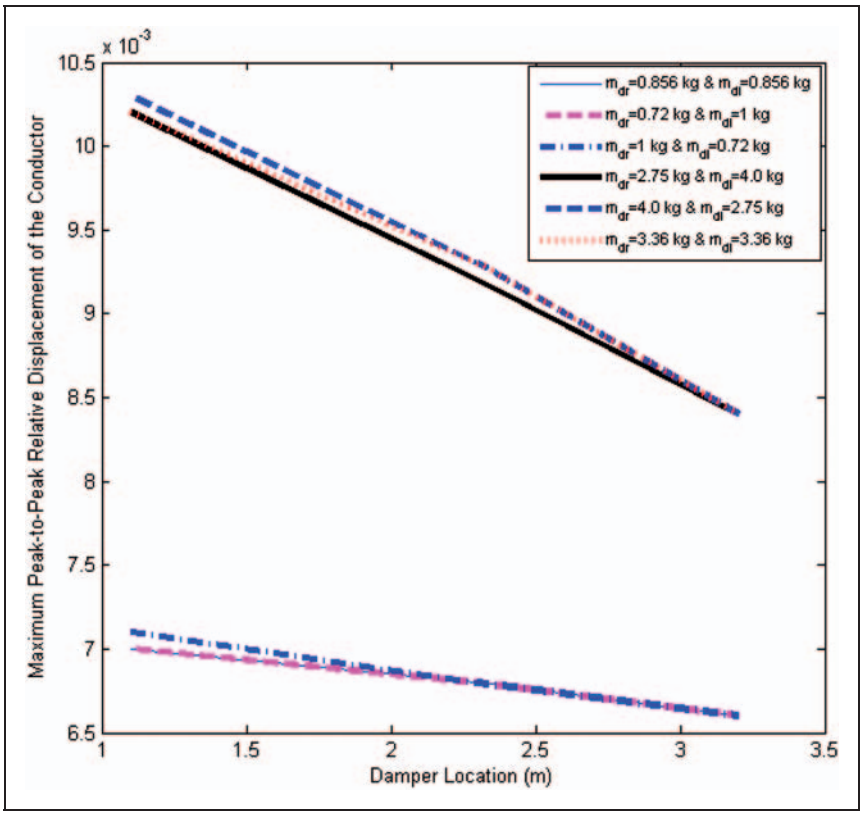

Figure 5. The effect of counterweight mass combinations on the normalized maximum peak-to-peak displacement of the conductor for $f = 9.53$ Hz.

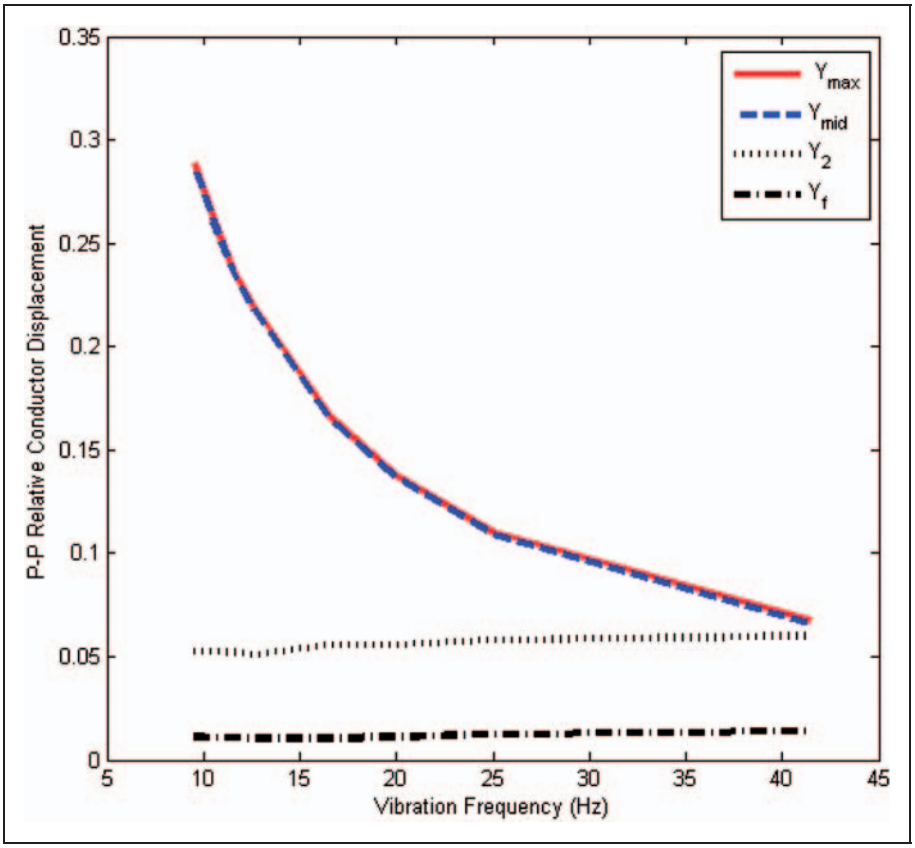

Figure 6. Variation of conductor peak-to-peak displacement with respect to excitation vibration frequency for $L_d = 0.898$ m.

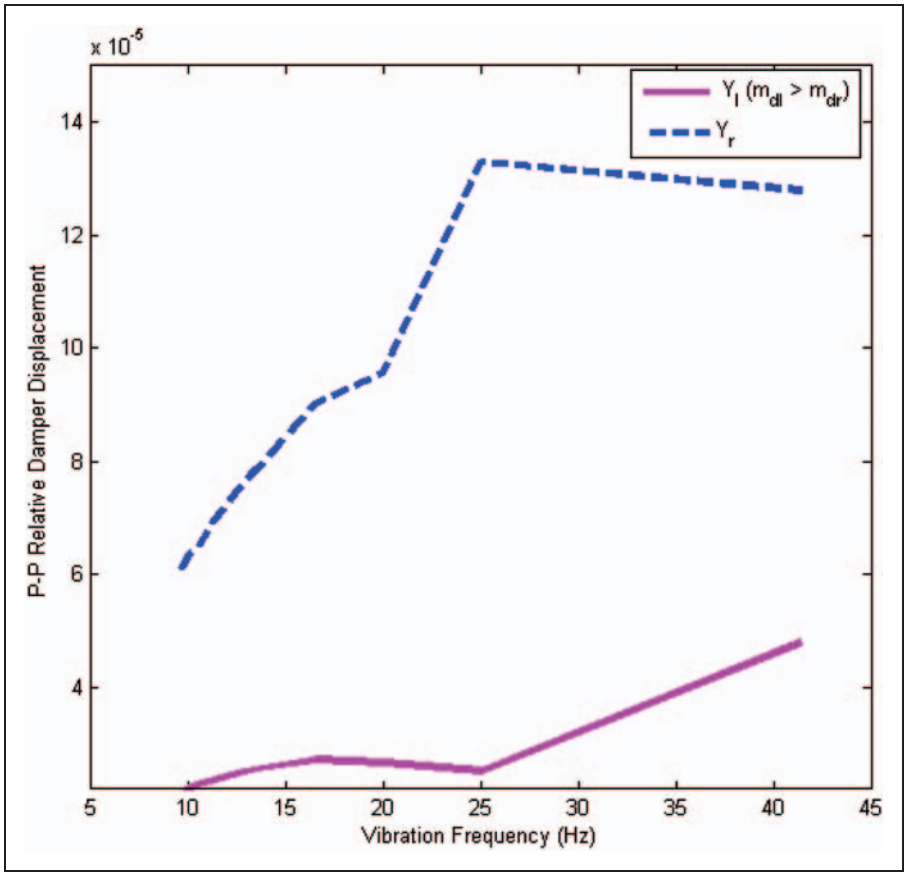

Figure 7. Variation of damper peak-to-peak displacement with respect to excitation vibration frequency for $L_d = 0.898$ m.

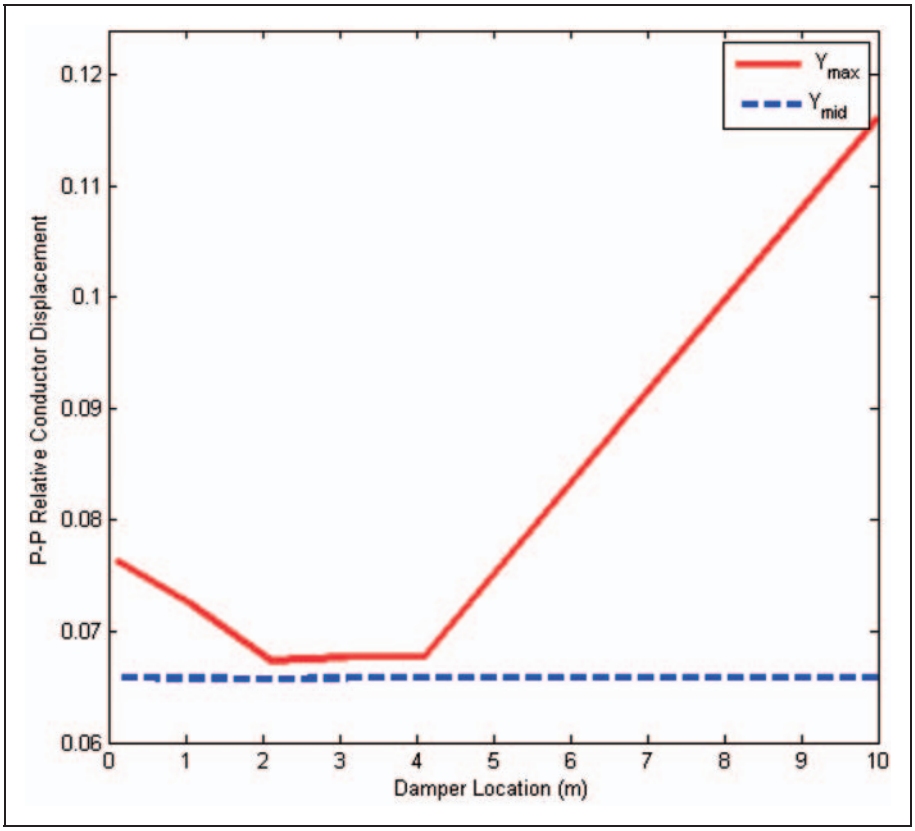

Figure 8. The conductor peak-to-peak displacement as a function of damper location for $f = 41.45$ Hz.

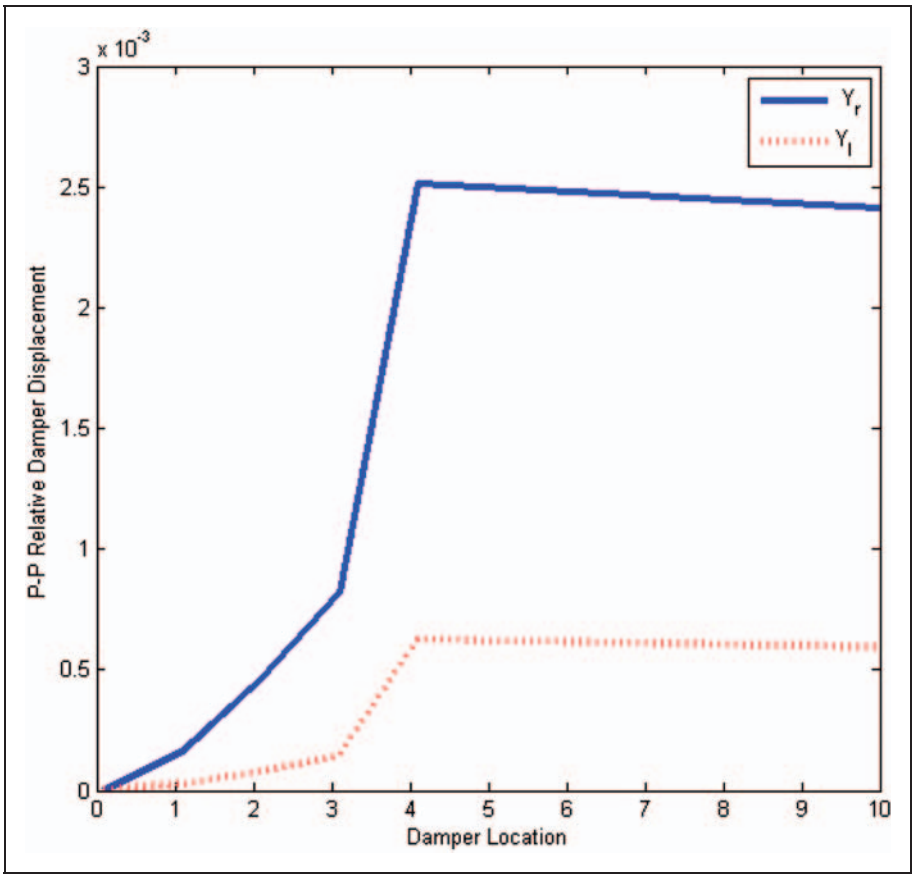

Figure 9. The damper peak-to-peak displacement as a function of damper location for $f = 41.45$ Hz.

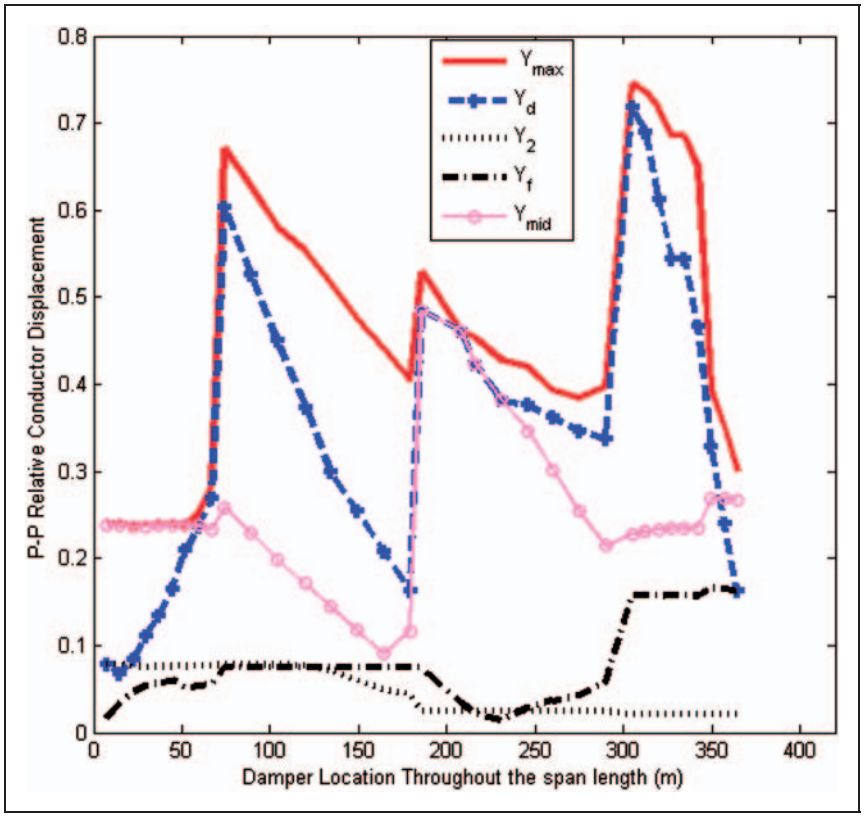

Figure 10. Variation of the conductor peak-to-peak displacement with respect to the damper location along the span length for $f = 10.10$ Hz.

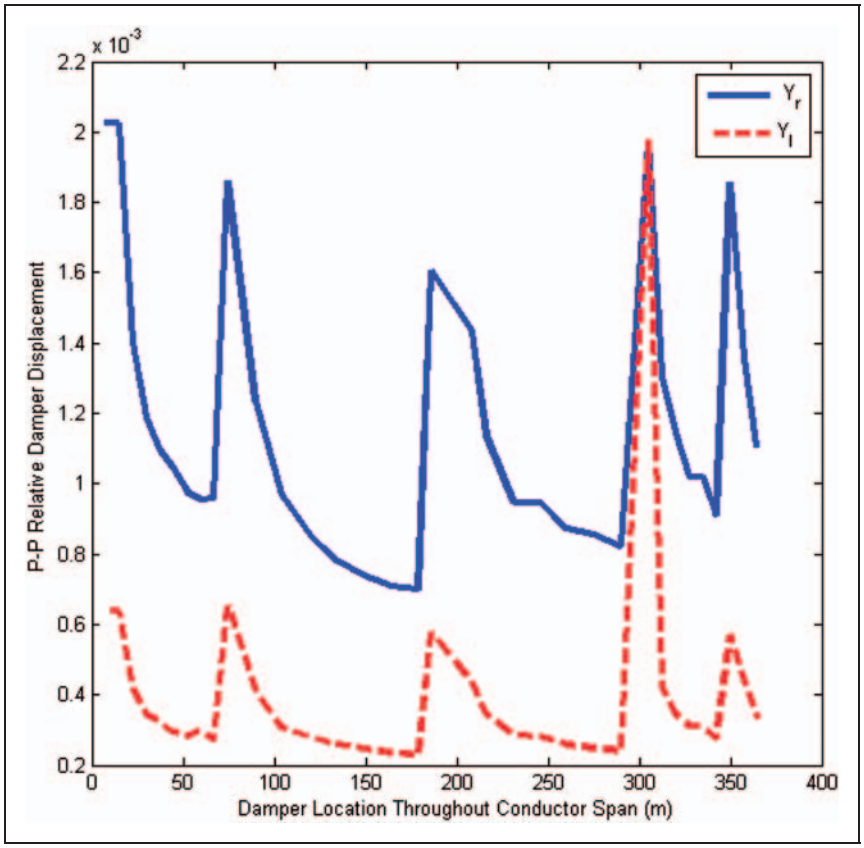

Figure 11. Variation of the damper peak-to-peak displacement with respect to the damper location along the span length for $f = 10.10$ Hz.

The variation of the peak-to-peak displacement of the damper counterweights, Y_{dr} and Y_{dl}, with the forcing frequency is shown in Figure 7 for $L_d = 0.898$. The damper vibration amplitude increases with the forcing frequency. This can be explained by noting that Stockbridge dampers dissipate the most energy at higher vibration frequencies. Generally, with respect to transmission lines, it can be concluded that vibration amplitude of the conductor decreases with increasing excitation frequency.

Effect of the damper location

The vibration response was investigated for various damper locations L_d while employing the previously listed damper properties. For an excitation frequency, f, of 41.45 Hz, the results in Figure 8 indicate that the optimum damper location range is from 2.2 to 4.1 m. This is slightly wider than the 2.4–3.6 m range reported by Nigol and Houston[5] for frequencies of 40–50 Hz and for longer spans and higher tension. The mid-span amplitude remains relatively constant compared to the maximum amplitude.

Figure 9 shows that the relative amplitude of both counterweights is maximum in the vicinity of the aforementioned damper location range. This is intuitive because the dissipation energy of the damper increases with the displacement of the damper.

To further improve the understanding of the effect of the damper location on the conductor motion, Figures 10 and 11, respectively, depict the conductor and damper counterweight displacements when the location of the damper is varied over the span of the conductor. The dampers are observed to be efficient only when they are located in the immediate vicinity of the span ends, closer to the tower.

Conclusion

A mathematical model has been proposed for the aeolian vibration analysis of a conductor with a Stockbridge damper. The model directly accounted for the two-way coupling between the conductor and damper. Hence, it permits the simultaneous assessment of the dynamic behaviors of the damper and the conductor. The following conclusions are inferred from the analyses.

1. The effectiveness of damper significantly depends on excitation frequency, the damper mass, and the location.
2. A damper is most efficient at higher vibration frequencies.
3. Asymmetric dampers are more efficient than symmetric dampers.
4. When using asymmetric dampers, it is preferable to position the counterweight with the larger mass nearer to the tower.
5. There is a damper location range that yields reducing maximum vibration amplitude of the conductor.

Funding

O. Barry was supported by the Natural Sciences and Engineering Research Council of Canada Postgraduate Scholarship and Ontario Graduate Scholarship.

References

1. EPRI. *Transmission line reference book: wind induced conductor motion*. Palo Alto, CA, 012317, 2006.
2. Claren R and Diana G. Mathematical analysis of transmission line vibration. *IEEE Trans Power Apparatus Syst* 1969; 60: 1741–1771.
3. Barbieri N, de Souza OH and Barbieri R. Dynamical Analysis of transmission lines cables: part1–linear theory. *Mecha Syst Sig Process* 2004; 18: 659–669.
4. Dhotard MS, Ganesan N and Rao BVA. Transmission line vibration. *J Sound Vib* 1978; 60: 217–237.
5. Nigol O and Houston HJ. Aeolian vibration of single conductor and its control. *IEEE Trans Power Apparatus Syst* 1985; 104: 3245–3254.
6. Krispin, HJ Optimization of the effciency of aeolian vibration dampers. *IEEE power Africa, conference and exposition*, Johannesburg, 16–20 July 2007.
7. Vecchiarelli, J. *Aeolian vibration of a conductor with a Stockbridge Type Damper*. PhD Thesis, University of Toronto, Canada, 1997.
8. Diana G, Falco M, Cigada A, et al. On The measurement of over head transmission lines conductor self-damping. *IEEE Trans Power Apparatus Sys* 2000; 15: 285–292.
9. Bishop R and Hassan A. The lift and drag forces on a circular cylinder oscillating in a flowing fluid. *Proc R Soc, London, Ser A* 1964; 277: 51–75.
10. Bearman PW and Currie IG. Pressure-fluctuation measurements on an oscillating circular cylinder. *J Fluid Mech* 1979; 91: 661–677.
11. Griffin O and Koopmann G. The vortex-excited lifts and reaction forces on resonantly vibrating cylinders. *J Sound Vib* 1977; 54: 435–448.
12. Hagedorn P. On the computation of damped wind-excited vibrations of overhead transmission lines. *J Sound Vib* 1982; 83: 253–271.
13. Hardy C and Noiseux DU. *Modeling of a single conductor-damper system response, Vol 1: Theoretical and validation manual*, Hydro Quebec, Montreal, Canada, 372 T 823, 1996 Canada: CEA.
14. Noiseux DU, Hardy C and Houle S. Statistical methods applied to aeolian vibration of overhead conductors. *J Sound Vib* 1987; 113: 245–255.
15. Tsui YT. Recent advances in engineering science as applied to aeolian vibrations an alternative approach. *Electr Power Sys res* 1982; 5: 73–85.
16. Barry, O. *Finite element modeling of a single conductor with a stockbridge damper under aeolian vibration*. MASc Thesis, Ryerson University, Canada, 2010.

Appendix

Components of the submatrices in equation (20)

$$\begin{aligned}\mathbf{M}_{cc} &= (\rho A)_c \int_0^{L_{ec}} \mathbf{N}_c \mathbf{N}_c^T d\xi \\ &+ m_{dr}\Big[\mathbf{N}_c^* \mathbf{N}_c^{*T} + L_{egr}(\mathbf{N}_c^* \mathbf{N}_c^{*'T} + \mathbf{N}_c^{'} \mathbf{N}_c^{*T} \\ &+ \mathbf{N}_c^{*'} \mathbf{N}_c^{*'T}(h^2 + L_{egr}^2))\Big] + I_{dr} \mathbf{N}_c^{*'} \mathbf{N}_c^{*'T} \\ &+ m_{dl}\Big[\mathbf{N}_c^* \mathbf{N}_c^{*T} - L_{egl}(\mathbf{N}_c^* \mathbf{N}_c^{*'T} \\ &+ \mathbf{N}_c^{'} \mathbf{N}_c^{*T} + \mathbf{N}_c^{*'} \mathbf{N}_c^{*'T}(h^2 + L_{egl}^2))\Big] \\ &+ I_{dl} \mathbf{N}_c^{*'} \mathbf{N}_c^{*'T} + m_{mr}\Big[\mathbf{N}_c^* \mathbf{N}_c^{*T} + \mathbf{N}_c^{'*} \mathbf{N}_c^{'*T} h^2\Big] \\ &+ \frac{1}{2}(\rho A)_{mr}\Big[L_{egr}^2(\mathbf{N}_c^* \mathbf{N}_c^{*'T} + \mathbf{N}_c^{*'} \mathbf{N}_c^{*T}) \\ &+ \frac{2}{3} L_{egr}^3 \mathbf{N}_c^{*'} \mathbf{N}_c^{*'T}\Big] \\ &+ m_{ml}\Big[\mathbf{N}_c^* \mathbf{N}_c^{*T} + \mathbf{N}_c^{'*} \mathbf{N}_c^{'*T} h^2\Big] \\ &+ \frac{1}{2}(\rho A)_{ml}\Big[-L_{egl}^2(\mathbf{N}_c^* \mathbf{N}_c^{*'T} \mathbf{N}_c^{*'} \mathbf{N}_c^{*T}) \\ &+ \frac{2}{3} L_{egl}^3 \mathbf{N}_c^{*'} \mathbf{N}_c^{*'T}\Big] d\xi\end{aligned}$$

$$\begin{aligned}\mathbf{M}_{cr} &= m_{dr}(\mathbf{N}_c^* \mathbf{N}_{dr}^{*T} + L_{egr} \mathbf{N}_c^{*'} \mathbf{N}_{dr}^{*T}) + I_{dr} \mathbf{N}_c^{*'} \mathbf{N}_{dr}^{*'T} \\ &+ (\rho A)_{mr} \int_0^{L_{egr}} (\mathbf{N}_c^* \mathbf{N}_{dr}^T + \xi_{mr} \mathbf{N}_c^{*'} \mathbf{N}_{dr}^T) d\xi_{mr} \\ \mathbf{M}_{rc} &= m_{dr}(\mathbf{N}_{dr}^* \mathbf{N}_c^{*T} + L_{egr} \mathbf{N}_{dr}^* \mathbf{N}_c^{*'T}) + I_{dr} \mathbf{N}_{dr}^{*'} \mathbf{N}_c^{*'T} \\ &+ (\rho A)_{mr} \int_0^{L_{egr}} (\mathbf{N}_{dr} \mathbf{N}_c^{*T} + \xi_{mr} \mathbf{N}_{dr} \mathbf{N}_c^{*'T}) d\xi_{mr} \\ \mathbf{M}_{cl} &= m_{dl}(\mathbf{N}_c^* \mathbf{N}_{dl}^{*T} - L_{egl} \mathbf{N}_c^{*'} \mathbf{N}_{dl}^{*T}) + I_{dl} \mathbf{N}_c^{*'} \mathbf{N}_{dl}^{*'T} \\ &+ (\rho A)_{ml} \int_0^{L_{egl}} (\mathbf{N}_c^* \mathbf{N}_{dl}^T - \xi_{ml} \mathbf{N}_c^{*'} \mathbf{N}_{dl}^T) d\xi_{ml} \\ \mathbf{M}_{lc} &= m_{dl}(\mathbf{N}_{dl}^* \mathbf{N}_c^{*T} - L_{egl} \mathbf{N}_{dl}^* \mathbf{N}_c^{*'T}) + I_{dl} \mathbf{N}_{dl}^{*'} \mathbf{N}_c^{*'T} \\ &+ (\rho A)_{ml} \int_0^{L_{egl}} (\mathbf{N}_{dl} \mathbf{N}_c^{*T} - \xi_{ml} \mathbf{N}_{dl} \mathbf{N}_c^{*'T}) d\xi_{ml}\end{aligned}$$

$$\begin{aligned}\mathbf{M}_{rr} &= m_{dr} \mathbf{N}_{dr}^* \mathbf{N}_{dr}^{*T} + I_{dr} \mathbf{N}_{dr}^{*'} \mathbf{N}_{dr}^{*'T} \\ &+ (\rho A)_{mr} \int_0^{L_{egr}} \mathbf{N}_{dr} \mathbf{N}_{dr}^T d\xi_{mr} \\ \mathbf{M}_{ll} &= m_{dl} \mathbf{N}_{dl}^* \mathbf{N}_{dl}^{*T} + I_{dl} \mathbf{N}_{dl}^{*'} \mathbf{N}_{dl}^{*'} T \\ &+ (\rho A)_{ml} \int_0^{L_{egl}} \mathbf{N}_{dl} \mathbf{N}_{dl}^T d\xi_{ml} \\ \mathbf{K}_{cc} &= (EI)_c \int_0^{L_{ec}} \mathbf{N}_c^{''} \mathbf{N}_c^{''T} d\xi - T \int_0^{L_{ec}} \mathbf{N}_c^{'} \mathbf{N}_c^{'T} d\xi \\ \mathbf{K}_{rr} &= (EI)_{mr} \int_0^{L_{egr}} \mathbf{N}_{dr}^{''} \mathbf{N}_{dr}^{''T} d\xi \\ \mathbf{K}_{ll} &= (EI)_{ml} \int_0^{L_{egl}} \mathbf{N}_{dl}^{''} \mathbf{N}_{dl}^{''T} d\xi\end{aligned}$$

where L_{ec}, L_{egr}, and L_{egl} denote the element length of the conductor, the right-side messenger, and the left-side messenger.

The prime on the shape functions represents the partial derivative with respect to ξ and

$$\begin{aligned}N_c^* &= N_c(L_c, t) \\ N_{dr}^* &= N_{dr}(L_{dr}, t) \\ N_{dl}^* &= N_{dl}(L_{dl}, t)\end{aligned}$$